

Timing and noise analysis of five millisecond pulsars observed with MeerKAT

M. Chisabi,¹★ S. Andrianomena,^{2,3}† U. Enwelum,⁴ E. G. Gasennelwe,⁵ A. Idris,⁵
 E. A. Idogbe,⁶ S. Shilunga,⁷ M. Geyer,^{8,2}‡ D. J. Reardon,^{9,10} C. F. Okany,^{6,11}
 M. Shamohammadi,^{9,10} R. M. Shannon,^{9,10} V. Venkatraman Krishnan,¹² F. Abbate,^{12,13}
 M. Kramer¹²

¹ Department of Physics, The Copperbelt University, Jambo Drive, Kitwe, 21696, Zambia

² SARA0, Liesbeek House, River Park Liesbeek Parkway, Settlers Way, Mowbray, Cape Town, 7705

³ Department of Physics & Astronomy, University of the Western Cape, Bellville, Cape Town 7535, South Africa

⁴ Department of Science Laboratory Technology, University of Nigeria, Nsukka

⁵ Department of Physics, University of Botswana, Gaborone, Botswana

⁶ National Space Research and Development Agency, Centre for Basic Space Science, Nsukka, 410102, Nigeria

⁷ Department of Physics, Chemistry and Material Science, University of Namibia, Private Bag 13301, Windhoek, Namibia

⁸ High Energy Physics, Cosmology & Astrophysics Theory (HEPCAT) Group, Department of Mathematics and Applied Mathematics, University of Cape Town, Rondebosch 7701, South Africa

⁹ Centre for Astrophysics and Supercomputing, Swinburne University of Technology, P.O. Box 218, Hawthorn, Victoria 3122, Australia

¹⁰ Australian Research Council Centre of Excellence for Gravitational Wave Discovery (OzGrav)

¹¹ Department of Physics & Astronomy, University of Nigeria, Nsukka, 410101, Nigeria

¹² Max-Planck-Institut für Radioastronomie, Auf dem Hügel 69, D-53121 Bonn, Germany

¹³ INAF - Osservatorio Astronomico di Cagliari, Via della Scienza 5, I-09047 Selargius (CA), Italy

Accepted XXX. Received YYY; in original form ZZZ

ABSTRACT

Millisecond pulsars (MSPs) in binary systems are precise laboratories for tests of gravity and the physics of dense matter. Their orbits can show relativistic effects that provide a measurement of the neutron star mass and the pulsars are included in timing array experiments that search for gravitational waves. Neutron star mass measurements are key to eventually solving the neutron star equation of state and these can be obtained by a measure of the Shapiro delay if the orbit is viewed near edge-on. Here we report on the timing and noise analysis of five MSPs observed with the MeerKAT radio telescope: PSRs J0900–3144, J0921–5202, J1216–6410, J1327–0755 and J1543–5149. We searched for the Shapiro delay in all of the pulsars and obtain weak detections for PSRs J0900–3144, J1216–6410, and J1327–0755. We report a higher significance detection of the Shapiro delay for PSR J1543–5149, giving a precise pulsar mass of $M_p = 1.349^{+0.043}_{-0.061} M_\odot$ and companion white-dwarf mass $M_c = 0.223^{+0.005}_{-0.007} M_\odot$. This is an atypically low mass measurement for a recycled MSP. In addition to these Shapiro delays, we also obtain timing model parameters including proper motions and parallax constraints for most of the pulsars.

Key words: pulsars: general – stars: neutron – astrometry – parallaxes

1 INTRODUCTION

Millisecond pulsars (MSPs) are recycled neutron stars that are typically found in binary systems (Bhattacharya & van den Heuvel 1991). The timing of periodic radio pulses emitted from MSPs allows for precise measurements of the properties of the pulsars

themselves and provides an opportunity for stringent tests of fundamental physics including searching for gravitational waves (Foster et al. 1990), testing theories of gravity (Kramer et al. 2021a), and constraining the neutron star equation of state through mass measurements (Cromartie et al. 2020). Through the detection of the Shapiro delay, a precise mass of the binary companion can be measured, and the neutron star (NS) mass inferred (Shapiro 1964). To date, the detection of Shapiro delay signatures have led to significant mass measurements in about 60 binary NS systems, ranging from $M_p \sim 1.2 M_\odot$ (Özel & Freire 2016) to the current most massive

★ E-mail: mukadichisabi@gmail.com

† E-mail: andrianomena@gmail.com

‡ E-mail: marisa.geyer@uct.ac.za

known NS, PSR J0740+6620, with $M_p = 2.08(7) M_\odot$ (Fonseca et al. 2021).

The measurements of the masses or radii of MSPs can strongly constrain the NS matter equation of state and, thus, the interior composition of neutron stars (e.g. Lattimer & Prakash 2004, 2007; Choudhury et al. 2024). Using X-ray data from NASA’s Neutron Star Interior Composition Explorer (NICER) instrument (Raaijmakers et al. 2021), onboard the International Space Station, astronomers have also determined the radius of PSR J0740+6620 to be $13.7^{+2.6}_{-1.5}$ and $11.36^{+0.95}_{-0.63}$ kilometres respectively (Miller et al. 2021; Choudhury et al. 2024). As constraints on the combination of mass and radius for more pulsars improve (e.g., Reardon et al. 2024), so too will our detailed understanding of the neutron star’s equations of state and its interior composition.

Finding pulsars with very high masses have the additional benefit that it allows for the exploration of matter on the verge of imploding to a black hole (Riley et al. 2021), ultimately probing the fundamental divide between neutron stars and black holes. A recent study using the MeerKAT telescope has identified a pulsar in a binary with another massive compact object. The mass of this companion lies within the range (previously considered a mass gap) between NSs and black holes; it remains uncertain whether the object is a NS or black hole (Barr et al. 2024). Such discoveries motivates continued analysis of NS masses via MSP binaries.

The sensitivity of a Shapiro delay detection and the resulting precision of a pulsar’s mass measurement depends on how precisely the MSP can be timed, and the magnitude of the delay signature, which is larger for binary systems viewed edge-on and with massive companions. Mass measurements are further enabled by the measurement of additional post-Keplerian parameters, such as the relativistic orbital precession (e.g. Serylak et al. 2022). Until recently, this meant that only the brightest MSPs with favourable alignments, or highly relativistic systems, lead to NS mass estimates via Shapiro delay measurements. With the increased timing sensitivity of the MeerKAT telescope (Parthasarathy et al. 2021; Spiewak et al. 2022) we now have the opportunity to turn to fainter or less studied MSPs in binary systems and attempt to constrain these NS masses. The MeerTime (Bailes et al. 2020) relativistic binary timing programme (Kramer et al. 2021b) uses the MeerKAT radio telescope in the Northern Cape province of South Africa with the aim to target many such systems.

In this work, we report on a search for Shapiro delay signatures in five MSPs observed as part of the MeerTime relativistic binary programme. The systems studied are all ideal MeerKAT targets in the Southern Sky, with declinations $\delta < -7$ deg. For all five pulsars, we describe their updated timing model parameters and noise properties.

In Section 2 we describe our observations from MeerKAT and summarise the data reduction pipeline. Section 3 describes the noise and timing model analysis using TEMPO2 and TEMPOEST, and Section 4 presents the results of this analysis. In Section 5 the results are discussed and compared with previous analyses, and the manuscript is concluded in Section 6.

2 OBSERVATIONS

For this work, we used MeerKAT data at L-band (856 – 1712 MHz) and UHF (544 – 1088 MHz) frequencies, obtained as part of the MeerTime Large Survey Project (LSP).

This includes data from the relativistic binary sub-theme within MeerTime. The relativistic binary sub-theme targets pulsars which

based on their known timing properties are candidate systems for new NS mass measurements via relativistic effects, or having NS masses already established are likely to provide estimates of post-Keplerian parameters through additional monitoring (for details see Kramer et al. 2021b). These targets are typically observed by conducting orbital campaigns of these sources at both L-band and UHF. Another MeerTime sub-theme, the MeerKAT Pulsar Timing Array (Miles et al. 2023, MPTA) programme, regularly conducts shorter timing observations of MSPs at L-band with the aim of searching for nanohertz-frequency gravitational waves (Spiewak et al. 2022; Miles et al. 2023). Here we utilise observations collected by both of these pulsar programmes.

MPTA observations have typical observing durations of 256 s (PSRs J0900–3144, J1216–6410 and J1543–5149), with some weaker pulsars observed for longer, to achieve $\sim 1 \mu\text{s}$ timing precision (i.e., observations of PSR J1327–0755 are typically 570 s). Observations of PSR J0921–5202 ranged from 256 s to 2045 s owing to a combination of MPTA observations and longer observing campaigns. For PSR J1543–5149, we include observations at UHF frequencies that were obtained as part of a dedicated observing campaign following our initial detection of a potential Shapiro delay signature. These data were taken as part of the MeerTime relativistic binary timing programme. In particular, a set of 18 UHF observations were scheduled, with a 2 hr observation coincident with the superior conjunction of the binary orbit, and two 1 hr observations either side of the superior conjunction, to maximise our sensitivity to the Shapiro delay signature. The remaining 13 UHF observations of ~ 30 min each were distributed across orbital phase.

The MeerKAT observations for each pulsar are summarised in Table 1. MeerKAT baselines for four out of the five pulsars span just over 4 years. One of the sources in this work, PSR J0921–5202, however, is no longer regularly monitored as part of the MPTA. Observing ceased because it produced poor timing precision and is therefore unlikely to contribute to the sensitivity of the MPTA to nanohertz-frequency gravitational waves. Only eight observations have been conducted for this pulsar with MeerKAT, which does not provide enough degrees of freedom to fit for the full timing model. We therefore also include published observations from the Murriyang, the 64-m radio telescope in Parkes, Australia, described by Lorimer et al. (2021a). This provided an additional 22 unique observations spanning 1.5 yrs (MJD 56767 to 57315) and extended the baseline of our analysed dataset to just over 6 yrs.

MeerKAT data from both receivers are recorded using the Pulsar Timing User Supplied Equipment (PTUSE) backend, which in its *fold-mode* records 8 second time integrations of filterbank data folded using a known pulse period and timing ephemerides, and produces 1024 phase bins across the pulse period (Bailes et al. 2020). The data are coherently dedispersed using a fiducial dispersion measure (DM) value with a frequency resolution of 1024 channels across the observing band, or ~ 0.8 MHz at L-band and ~ 0.5 MHz for UHF.

The data are processed using the MEERPIPE¹ data reduction pipeline. In this pipeline, the data are summed in polarisation to total intensity, reduced to eight (L-band) or nine (UHF) frequency channels and between five and nine time sub-integrations, depending on the pulsar and observing length. Template pulse profiles were generated using the PSRCHIVE (Hotan et al. 2004) wavelet smoothing algorithm on a high signal-to-noise ratio pulse profile produced from summing all of the observations. The template profile retained

¹ <https://github.com/OZGrav/meerpipe>

the same number of channels as the observations to allow each channel to be timed against an appropriate template, accounting for profile evolution across the observing band. The times-of-arrival (ToAs) per frequency sub-band and per time sub-integration were then computed using these templates and the Fourier-domain Monte Carlo algorithm from `PSRCHIVE`. As part of the subsequent timing analysis we removed ToAs for which the associated pulse profile had a signal-to-noise ratio less than 10.

3 METHODS

3.1 Timing and noise models

We use standard timing and noise modelling techniques to establish robust timing model parameters. The ToAs are compared to timing models that describe the spin evolution and astrometric properties of the pulsar, the orbit if it has a binary companion and the line-of-sight propagation through the ionised interstellar medium (ISM). Relativistic corrections to the pulse propagation through the surrounding curved space-time, in the case of a binary system, can also be modelled, enabling measurements of the pulsar and companion masses. Arrival times were corrected from an observatory time standard to the BIPM(2021) realisation of International Atomic Time². Thereafter, arrival times were transformed to the solar system barycentre using the DE440 Solar System ephemeris as obtained from the Jet Propulsion Laboratory (JPL; Park et al. 2021). For all pulsars, except PSR J1327–0755 as discussed in Sec. 4.4, we assume the default line-of-sight solar wind electron density of $n_e = 4 \text{ cm}^{-3}$.

The parameters describing the timing model undergo a least-squares fit of the linearised model to the measured ToAs using `TEMPO2` (Edwards et al. 2006). The difference between the observed ToAs and those predicted by the pulsar timing model are the *timing residuals*. The timing residuals contain the latent measurement errors, pulse jitter, timing noise (e.g. Shannon & Cordes 2010), and any unmodeled physical or instrumental processes. These noise processes need to be modeled to enable a robust generalised least-squares fit of the timing model parameters, which returns reliable parameter uncertainty estimates.

We use the “ELL1” binary model appropriate for the near-circular orbits of the pulsars in our sample (Lange et al. 2001). This model ignores orbital perturbations that depend on terms with eccentricity (e) of the order e^2 or higher. We confirm that these additional delays, $\delta t_{\text{ell1}} \sim 0.5xe^2$, for x the projected semi-major orbital axis, are much smaller than the weighted root-mean-square timing residual for each pulsar we studied. We also include, for all pulsars an “FD” parameter that models residual frequency-dependent delays caused, for example, by profile template errors (Zhu et al. 2015).

3.2 Noise modelling

We use `TEMPO2` (Lentati et al. 2014) to characterise the pulsar timing model while simultaneously assessing for the presence, and modelling the effect of, additional stochastic noise processes. `TEMPO2` can conduct a simultaneous Bayesian analysis of the linear or non-linear deterministic pulsar timing model and additional stochastic parameters. It uses the Bayesian inference nested

sampler `MULTINEST`³ to efficiently explore the noise model parameter space (Feroz et al. 2009). We also use `TEMPO2` to sample over the timing model parameters of most importance for this work, which are those describing the curved spacetime, and the pulsar timing parallax, while analytically marginalising over other parameters using the design matrix derived from a `TEMPO2` fit.

The noise model includes known stochastic processes, such as white noise processes to account for pulse jitter, dispersion measure variations, and achromatic red noise. Within the `TEMPO2` framework the stochastic white noise processes are defined by the parameters, EFAC, EQUAD and ECORR. The EFAC, F , parameters apply a scaling factor per observing backend to all ToA uncertainties to account for errors arising from the template matching procedure by which the ToA uncertainties were obtained. The EQUAD, Q , parameter is a secondary white noise parameter, which accounts for an independent source of noise, added in quadrature to the scaled ToA uncertainties. The modified uncertainty, σ_{mod} , depends on the original uncertainty, σ_{TOA} , as $\sigma_{\text{mod}} = \sqrt{(F\sigma_{\text{TOA}})^2 + Q^2}$ (Lentati et al. 2014). Finally the ECORR parameter describes a process that is also added in quadrature but that is fully correlated in frequency for multi-band ToAs, but independent in time (NANOGrav Collaboration et al. 2015). It therefore captures, for example, frequency dependent profile errors weighted by flux density variations from scintillation, pulse jitter, or propagation effects within a given observing epoch.

Slow varying changes in (observing frequency-dependent) DM values are modeled by a long-term time correlated noise process, with its power spectral density (PSD) described by a power law, and a Fourier basis for which the number of Fourier frequency components are modeled to a maximum frequency of $1/30 \text{ days}^{-1}$, or roughly twice our observing cadence. An additional red noise process, with a similar PSD, is also modeled to account for either spin irregularities in the pulsars, or for contributions from the putative stochastic gravitational-wave background (Agazie et al. 2023; EPTA Collaboration et al. 2023; Reardon et al. 2023a; Xu et al. 2023). These power law PSDs are described by the parameters DMamp, DMSlope and RNamp and RNSlope in `TEMPO2` respectively.

In our analysis we include all noise model parameters for all pulsars. We quantify the data-driven Bayesian support for each of these processes via the Savage-Dickey (SB) density ratio, which gives an estimate of the Bayes factor (BF, or \mathcal{B}) for each process (see Arzoumanian et al. 2018b). This Bayes factor is calculated by comparing the posterior support for a noise process in the weak signal regime to the prior density.

3.3 Searching for Shapiro delays

The Shapiro delay (Shapiro 1964) is the retardation of the pulse arrival times from a pulsar when pulses propagate through the compressed space-time associated with a binary companion. The Shapiro delay varies over binary orbital phase, with the largest delay observed during superior conjunction when the pulsar is directly behind its companion. The Shapiro delay can be characterised by two parameters, the range,

$$r = T_{\odot} M_c \quad (1)$$

and shape

$$s = \sin i, \quad (2)$$

² <https://websites.bipm.org/ftp/pub/tai/ttbipm/TTBIPM.2021>

³ <http://ccpforge.cse.rl.ac.uk/gf/project/multinest/>

Table 1. MeerKAT and Murriyang timing baselines and number of generated times-of-arrival (ToAs) at L-band and UHF frequencies as used in this work.

Pulsar name	J0900–3144	J0921–5202	J1216–6410	J1327–0755	J1543–5149
Telescope/Backend: <i>MeerKAT/PTUSE</i>					
Number of ToAs at L-band	1105	128	816	595	1010
Number of ToAs at UHF	216	–	72	–	1757
Number of observations at L-band	89	30	86	70	89
Number of observations at UHF	3	–	2	–	18
Date range (MJD)	58595 – 60116	58623 – 59086	58557 – 60116	58855 – 60123	58595 – 60116
Telescope/Backend: <i>Murriyang/MultiBeam</i>					
Number of ToAs at 1382 MHz	–	22	–	–	–
Number of observations at 1382 MHz	–	22	–	–	–
Date range (MJD)	–	56767 – 57315	–	–	–

where M_c is the mass of the companion, i the inclination of the orbit on the sky, and $T_\odot = GM_\odot/c^3 = 4.925490947 \mu\text{s}$ is the mass of the Sun in units of time.

These Shapiro delay quantities can alternatively be expressed in terms of pair of orthometric parameters (Freire & Wex 2010), namely the harmonic amplitude (h_3)

$$h_3 = T_\odot M_c \zeta^3, \quad (3)$$

and ratio (ζ)

$$\zeta = \frac{\sin i}{1 + |\cos i|}. \quad (4)$$

It is particularly advantageous to search for Shapiro delay signatures in approximately circular binaries using this less covariant parameterization. For each pulsar analysed here we have low values of eccentricity and therefore search for Shapiro delays by sampling the orthometric parameters in TEMPO_{NEST}, simultaneously with the noise model. Once obtained from Bayesian inference, the Shapiro delay parameters (h_3 , ζ) are used to estimate the mass of the companion (M_c) and the orbital inclination (i) from equations 3 and 4, while the pulsar mass is derived using the mass function,

$$\frac{(M_c \sin i)^3}{(M_p + M_c)^2} = \frac{4\pi^2 x_p^3}{T_\odot P_b^2}, \quad (5)$$

with P_b and x_p the orbital period and the projected semi-major axis respectively, and $T_\odot = \frac{GM_\odot}{c^3} = 4.925490947 \mu\text{s}$.

4 RESULTS

We discuss the characteristics and analysis for each MSP independently, reporting updated timing parameters and properties of the preferred noise models for each. For all pulsars (except PSR J0921–5202 for which we have very little data) we evaluated evidence for white noise, red noise and DM noise processes as discussed in Sec 3.2. We include white noise parameters for all studied systems, and DM and Red-noise parameters where we find sufficient evidence for them as assessed using Savage-Dickey density ratios. We also searched for parallax and Shapiro delay parameters, h_3 and ζ for all pulsars. A summary of the obtained timing parameters is presented in Table 2.

4.1 PSR J0900–3144

PSR J0900–3144 was discovered in the Parkes high-latitude pulsar survey (Burgay et al. 2006). It continues to be regularly monitored

by the European Pulsar Timing Array (EPTA) programme. A previous timing analysis of this pulsar was conducted using 7 years of observations from the EPTA (Desvignes et al. 2016). The pulsar is also observed by the Parkes Pulsar Timing Array and a noise analysis has been conducted (Reardon et al. 2023b).

Using 2 years and 9 months of observations from MeerKAT, we detect significant dispersion measure variations, $DM(t)$ and also find strong evidence for red noise as shown in the top left panel in Figure 1. During an initial inspection of the timing residuals using a timing model that was fitted to the first ~ 2 yrs of data without accounting for red noise, we identified structure in the residuals that resembles a weak pulsar glitch occurring near the beginning of 2023. Although rare, glitches have been observed in millisecond pulsars (McKee et al. 2016; Cognard & Backer 2004). Using TEMPO_{NEST}, we searched for glitch parameters in this pulsar, but found no significant evidence compared with a model of just red noise. We find an insignificant Bayes Factor ($\ln \mathcal{B} = 1.1$, inferred by comparing the evidences computed with nested sampling) for the model with both red noise and a glitch relative to a model of only red noise. The inferred glitch amplitude, corresponding to a change in spin frequency, is $(1.5 \pm 0.7) \times 10^{-10}$ Hz. Using our data we therefore conclude that the appearance of glitch-like residuals may be due to stochasticity in the red noise and that additional data is required to confirm or refute a glitch.

We find only weak evidence for correlated noise (ECORR) in the L-band observing system, with a Savage-Dickey density ratio of $SD = 1.3$, but no evidence for correlated noise at UHF ($SD = 0.69$). Our best-fitting timing residuals, after subtracting the characterised noise processes, are plotted in the top right panel of Figure 1.

When we searched for a Shapiro delay we were able to constrain h_3 , as reported in Table 2, but unable to constrain ζ . We are therefore neither able to constrain the pulsar mass or orbital inclination for PSR J0900–3144. We report a marginal detection of timing parallax of $\varpi = 0.47^{+1.04}_{-0.41}$ mas.

We measure a proper motion of $\mu_\alpha = -1.2(5)$ mas yr⁻¹ in right ascension and $\mu_\delta = 1.8(5)$ mas yr⁻¹ in declination. In Desvignes et al. (2016) the authors present proper motions of $\mu_\alpha = -1.01(5)$ mas yr⁻¹ and $\mu_\delta = 2.02(7)$ mas yr⁻¹. These measurements are consistent with ours, however the earlier measurements of Desvignes et al. (2016) are much more precise given their longer data span of almost 7 years. Our astrometry is also consistent with Shamohammadi et al. (2024) which presented astrometry from a nearly identical MeerKAT data set for this pulsar.

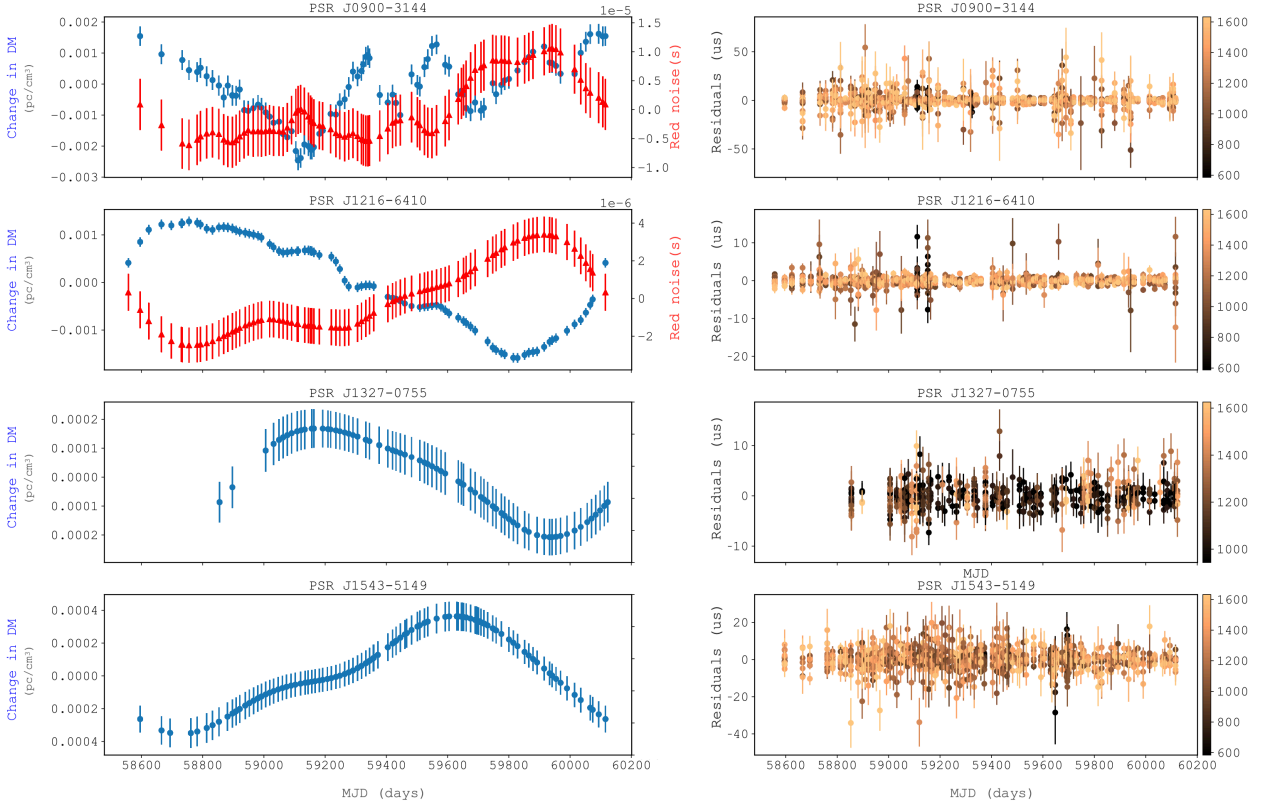


Figure 1. *Left column:* Variations in dispersion measure values (in pc cm^{-3} , in blue) and timing residuals due to red noise (in s , in red) across observing days, for the pulsars in our sample for which we found evidence for DM and/or Red noise. The plotted noise model for PSR J1543-5149 does not include red noise since it is poorly constrained with only modest support (see Table 2). *Right column:* Noise subtracted residuals (in μs) for our data sets. Each marker is coloured according to the frequency bin (which is denoted by the colour bar) it belongs to. The observations of PSR J1543-5149 (bottom row) include both L and UHF-bands.

4.2 PSR J0921–5202

This target was first discovered in archival data from the Parkes Multibeam Pulsar Survey (Mickaliger et al. 2012). A timing analysis spanning approximately 3 years followed using Murriyang (Lorimer et al. 2021b). From this analysis the authors placed an upper limit on the total proper motion for PSR J0921–5202 of $< 216 \text{ mas yr}^{-1}$. In our analysis, we use the available MeerKAT L-band data (taken between 2019 May 20 and 2020 Aug 24), to which we add $\sim 1.5\text{yr}$ historic Murriyang data. We account for the constant timing offsets between these data sets by including an additional jump parameter in TEMPO2. We find no evidence for DM, red or correlated white noise in our data set, and therefore only include the white noise parameters EFAC and EQUAD in our analysis. We also do not find any evidence for parallax. We measure proper motions for this pulsar for the first time, finding $\mu_\alpha \cos \delta = -5.2(1.8) \text{ mas yr}^{-1}$ in right ascension and $\mu_\delta = 8.8(1.7) \text{ mas yr}^{-1}$ in declination, which provides a total proper motion of $\mu_T = 10.22(18) \text{ mas yr}^{-1}$.

4.3 PSR J1216–6410

This pulsar was first discovered during the Parkes Multibeam Pulsar Survey (PMPS, Lorimer et al. 2006). It has the tightest orbit of our analysed sample, with an orbital period of 4.04 days. As part of the

PMPS, PSR J1216–6410 was observed for 2.1 years. With 3.2 years of total observing time using the MeerKAT L-band, we measure a proper motion of $\mu_\alpha = -7.87(8) \text{ mas yr}^{-1}$ in right ascension and $\mu_\delta = 2.57(8) \text{ mas yr}^{-1}$ in declination, which provides a total proper motion of $\mu_T = 8.28(8) \text{ mas yr}^{-1}$. We furthermore obtain a parallax measurement of $\varpi = 1.14^{+0.46}_{-0.44} \text{ mas}$, which translates to a distance estimate of $0.88^{+0.55}_{-0.23} \text{ kpc}$, when using $1/\varpi$ as the conversion. These are consistent with the astrometry presented in Shamohammadi et al. (2024).

We find clear evidence for both a DM noise process and a red noise process in our dataset, but no evidence for jitter noise (all ECORR parameters have SD ratios below 0.7). We note that the maximum likelihood time-domain realisations of the DM and red noise processes in Figure 1 are anti-correlated. This can arise because of other unmodelled chromatic red processes, such as scattering variations (Lentati et al. 2016). However, since our noise model whitens the timing residuals sufficiently to provide accurate timing model measurements, we defer a detailed examination of the noise processes in this pulsar to future work.

We are able to constrain the amplitude of h_3 , as indicated in Table 2, but not ζ .

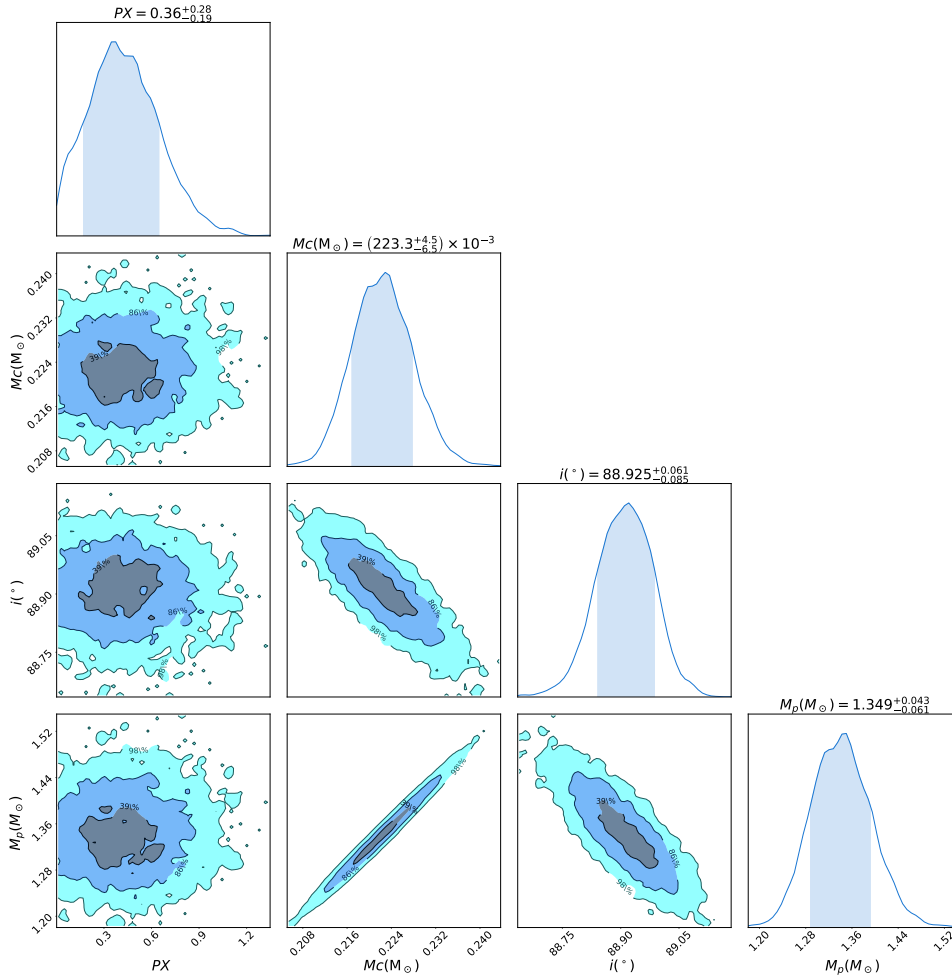


Figure 2. Posterior distributions for a subset of timing parameters of PSR J1543–5149. Here we show parallax (PX) as well as mass of the companion (M_c) and pulsar (M_p) and the inclination angle of the binary. Note that the sense of the inclination angle is not established, therefore $180^\circ - i$ is an equally likely estimate to the value of i presented here.

4.4 PSR J1327–0755

PSR J1327–0755 was discovered as part of a drift scan undertaken by the Green Bank Telescope (GBT) at 350 MHz while immobilized during track refurbishments (Boyles et al. 2013). Using 70 observations, and over 3.5 years of observation at MeerKAT L-band, we detect a parallax of $\varpi = 0.66 \pm 0.22$ mas. This measurement deviates from the weak detection ($\varpi = 0.13^{+0.17}_{-0.09}$ mas) presented in Shamohammadi et al. (2024), but is more consistent with the DM distance estimate from the NE2001 Galactic electron density model which predicts, $D = 1.73$ kpc (Cordes & Lazio 2002), while (Yao et al. 2017) places the pulsar much more distant $D = 25$ kpc. The discrepancy between our measurement and Shamohammadi et al. (2024), likely stems from our longer time span (3.5 yr compared to their 2.4 yr), allowing us to obtain a more accurate ϖ estimate.

We measure a proper motion of $\mu_\alpha = -2.5(1.2)$ mas yr $^{-1}$ in right ascension and $\mu_\delta = 7.5(2.9)$ mas yr $^{-1}$ in declination, consistent with the measurements reported in Shamohammadi et al. (2024). We searched for a Shapiro delay, and constrained only h_3 very weakly.

We find moderate evidence for dispersion measure variations as captured in the DM noise parameters in Table 2, with a SD density

ratio of 6.7 and find no evidence for a red noise process (SD density of 0.7).

This pulsar has a low ecliptic latitude (1.2 degrees) and is therefore more sensitive to variations in the solar wind than the other pulsars in our sample. For this reason, we fit for the mean solar wind electron density at a distance of 1 AU, and find $n_e = 6.7 \pm 0.6$ cm $^{-3}$. This mean density is used to compute the dispersive time delays due to the solar wind at each observing epoch, assuming a spherically-symmetric n_e distribution (Edwards et al. 2006).

4.5 PSR J1543–5149

PSR J1543–5149 was discovered as part of the High Time Resolution Universe (HTRU) survey for pulsars and fast transients carried out from 2008 with Murriyang (Keith et al. 2011).

The pulsar, with its spin period of 2.06 ms, is the fastest spinning pulsar in our data set. It has an orbital period of 8.06 days and was first detected with a S/N of 16 in a Murriyang observation offset 0.08° from the nominal pulsar position. It is in a binary system with a white dwarf companion that has a minimum companion mass of $0.22 M_\odot$, making it a low-mass pulsar binary (Keith et al. 2011).

MeerKAT observed PSR J1543–5149 for 6.4 hrs in the L-band, as well as 1.3 hrs in UHF. We detected significant DM variations

Table 2. Timing parameters for our pulsar sample. We assume the DE440 solar system ephemeris and the BIPM2021 time standard for all pulsars. Symmetric errors are presented in parentheses and apply to the last quoted decimal place, whereas asymmetrical errors as obtained from Bayesian posterior analysis or Monte Carlo simulation are explicitly stated. All uncertainties represent 1σ , 68% confidence interval. The transverse velocities[†] are derived using our measured pulsar distance, where available, or with a distance estimate (with 20% error bar) from a Galactic electron density model (Yao et al. 2017) otherwise.

Pulsar	J0900–3144	J0921–5202	J1216–6410	J1327–0755	J1543–5149
Observation and reduction parameters					
Solar System ephemeris	DE440	DE440	DE440	DE440	DE440
Time standard	TT(BIPM2021)	TT(BIPM2021)	TT(BIPM2021)	TT(BIPM2021)	TT(BIPM2021)
Reference epoch (MJD)	59157	57926	59143	59292	59163
Solar wind electron density, n_e (cm ⁻³)	4	4	4	6.7(6)	4
Spin and astrometric parameters					
Period and position epoch	59157	57926	59143	59292	59163
Right ascension, α (J2000, h:m:s)	09:00:43.95221(5)	09:21:59.8780(6)	12:16:07.321166(14)	13:27:57.58064(9)	15:43:44.145260(10)
Declination, δ (J2000, d:m:s)	-31:44:30.8723(7)	-52:02:38.448(5)	-64:10:09.16646(10)	-07:55:29.912(4)	-51:49:54.71366(16)
Proper motion in α , μ_α (mas yr ⁻¹)	-1.2(5)	-5.2(18)	-7.87(8)	-2.5(1.2)	-3.96(8)
Proper motion in δ , μ_δ (mas yr ⁻¹)	1.8(5)	8.8(18)	2.57(8)	8(3)	-2.36(13)
Parallax, ϖ (mas)	0.47 ^{+1.04} _{-0.41}	–	1.14 ^{+0.46} _{-0.44}	0.66(22)	0.36 ^{+0.28} _{-0.19}
Spin frequency, ν (Hz)	90.011841777132(10)	103.30777266468(4)	282.535701428469(7)	373.423698381884(5)	486.154230881221(9)
Spin-down rate, $\dot{\nu}$ (10 ⁻¹⁶ Hz s ⁻¹)	-3.954(6)	-1.928(7)	-1.276(4)	-2.519(3)	-3.8205(5)
Dispersion measure, DM (cm ⁻³ pc)	75.6866(3)	122.711(3)	47.39301(15)	27.9084(5)	50.98325(12)
Binary model parameters					
Model name	ELL1H	ELL1	ELL1H	ELL1H	ELL1H
Orbital period, P_b (days)	18.7376360567(17)	38.22367666(11)	4.03672725263(11)	8.4390861450(5)	8.0607731359(5)
Projected semi-major axis, x_p (lt-s)	17.24880847(18)	19.053379(6)	2.93709185(6)	6.64577327(13)	6.48028675(8)
Epoch of ascending node T_{asc}	52678.6302890(7)	56769.836938(4)	53055.36126059(16)	54717.3832595(3)	54929.0678258(3)
First Laplace-Lagrange parameter, ϵ_1	9.86(3)×10 ⁻⁶	-8.9(8)×10 ⁻⁶	1.6(4)×10 ⁻⁷	-7.6(36)×10 ⁻⁸	2.047(3)×10 ⁻⁵
Second Laplace-Lagrange parameter, ϵ_2	3.50(3)×10 ⁻⁶	1.11(8)×10 ⁻⁵	-5.61(4)×10 ⁻⁶	-4.6(36)×10 ⁻⁸	6.010(20)×10 ⁻⁶
Noise parameters					
DM noise amplitude (log ₁₀ A _{DM})	-10.857 ^{+0.069} _{-0.067}	–	-11.247 ^{+0.085} _{-0.076}	-11.78 ^{+0.36} _{-0.60}	-11.54 ^{+0.40} _{-0.20}
DM noise spectral index	1.65 ^{+0.20} _{-0.27}	–	3.10 ^{+0.40} _{-0.39}	3.1 ^{+1.9} _{-1.2}	2.42 ^{+0.59} _{-1.95}
Red noise amplitude (log ₁₀ A _{Red})	-12.143 ^{+0.062} _{-0.109}	–	-12.87 ^{+0.11} _{-0.17}	–	-13.34 ^{+0.58} _{-0.89}
Red noise spectral index	2.58 ^{+0.42} _{-0.49}	–	3.87(86)	–	4.01 ^{+1.20} _{-1.69}
Weighted timing residual, w_{rms} (μ s)	7.768	23.7	1.805	1.507	2.304
Weighted residuals noise-subtracted w_{rms} (μ s)	1.960	–	0.774	1.421	1.685
Shapiro delay, mass and inclination measurements					
Orthometric amplitude, h_3 (10 ⁻⁷ s)	4.6 ^{+1.6} _{-1.5}	–	0.71 ^{+0.36} _{-0.39}	0.97 ^{+0.91} _{-0.65}	10.4 ^{+0.19} _{-0.26}
Orthometric ratio, ζ	–	–	–	–	0.9814 ^{+0.0011} _{-0.0015}
Orbital inclination, i (deg)	–	–	–	–	88.925 ^{+0.061} _{-0.085}
Companion mass, M_c (M_\odot)	–	–	–	–	0.2233 ^{+0.0045} _{-0.0065}
Pulsar mass, M_p (M_\odot)	–	–	–	–	1.349 ^{+0.043} _{-0.061}
Derived parameters					
Total proper motion, μ_T (mas yr ⁻¹)	2.2(5)	10.22(18)	8.28(8)	8(3)	4.61(14)
Spin period, P_0 (ms)	11.109649355648(1)	9.679813766248(4)	3.53937571409245(90)	2.67792323929411(4)	2.05696039750053(4)
Spin period derivative, \dot{P} (10 ⁻²⁰ s s ⁻¹)	4.880(8)	1.807(7)	0.1598(5)	0.1806(3)	0.16165(2)
Distance estimate ($1/\varpi$, kpc)	–	–	0.88 ^{+0.55} _{-0.23}	1.5 ^{+0.8} _{-0.4}	2.8 ^{+3.1} _{-1.6}
Dispersion distance (kpc)	0.38	0.36	1.10	<25	1.15
Transverse velocity [†] (v_\perp , km/s)	4	17	34 ⁺²² ₋₉	57 ⁺³⁰ ₋₁₅	61 ⁺⁶⁸ ₋₃₅

as shown in the bottom panel of Figure 1, but no correlated noise (ECORR) in either the L-band or UHF band observing systems. We find modest evidence for red noise, with an estimated SD ratio of 2.3. We find no significant parallax for this pulsar.

We detect a Shapiro delay signature for PSR J1543–5149, with measured values $h_3 = 1.04^{+0.19}_{-0.25} \mu$ s and $\zeta = 0.9814^{+0.0011}_{-0.0015}$. This allows us to constrain the mass of the pulsar to $M_p = 1.349^{+0.043}_{-0.061} M_\odot$, the companion mass to $M_c = 0.2233^{+0.0011}_{-0.0015} M_\odot$, and the orbital inclination angle to $i = 88.925^{+0.061}_{-0.085}$ degrees. It is because of this near edge-on orbital orientation that we are able to clearly distinguish the Shapiro-delay signature for this pulsar. The posterior

probability distributions of h_3 and ζ , as well as M_c , M_p , and i that are derived from h_3 and ζ , are plotted in Figure 2.

We measure a proper motion of $\mu_\alpha = 3.85 \pm 0.12$ mas yr⁻¹ in right ascension and $\mu_\delta = -2.86 \pm 0.18$ mas yr⁻¹ in declination. Our measurement of μ_α is in modest ($\approx 1\sigma$) disagreement with the value presented in Shamohammadi et al. (2024), likely because of different noise models. We also find evidence for a parallax measurement, obtaining $\varpi = 0.36^{+0.28}_{-0.19}$ mas, as presented in Figure 2, and consistent with Shamohammadi et al. (2024). This mildly constrained value leads to a distance estimate of PSR J1543–5149 of $2.8^{+3.1}_{-1.6}$ kpc, when using $1/\varpi$. All additional measured timing model parameters including proper motion are shown in Table 2.

5 DISCUSSION

5.1 The low mass of PSR J1543–5149

Our inferred mass of $M_p = 1.349^{+0.043}_{-0.061}$ is unusually low for a recycled MSP. There are only five known MSPs with mass measurements constrained to be below $M_p = 1.4 M_\odot$ with at least 1σ significance. The other MSPs (defined as $\nu > 100$ Hz) with such masses are PSRs J0514–4002A, J1807–2500B, J1918–0642 and J2234+0611 (Ridolfi et al. 2019; Lynch et al. 2012; Arzoumanian et al. 2018a; Stovall et al. 2019). These pulsars are mostly in eccentric orbits (PSR J2234+0611) or in orbits formed through exchange encounters in a globular cluster (PSRs J0514–4002A and J1807–2500B) and as such their masses can depend on a complex evolutionary history. PSRs J1918–0642 and J1543–5149 stand out among these low-mass MSPs as they are in standard highly circular orbits with a Helium white-dwarf companion and are likely to have formed through the most common MSP evolution channel. PSR J1918–0642, while centered a lower mass value of $M_p = 1.29^{+0.10}_{-0.09}$ has a less precise measurement than our measurement for PSR J1543–5149. We estimate the accreted mass during this MSP evolution to be $\Delta M \sim 0.1 M_\odot$ from Equation 14 of Tauris et al. (2012), suggesting a birth neutron star mass of $M_p \sim 1.25 M_\odot$.

5.2 Pulsar and companions mass estimates

For each pulsar with a weak detection of Shapiro delay (significant h_3 only), PSRs J0900–3144, J1216–6410, and J1327–0755, we use the numerical model prescribed in Shamohammadi et al. (2022) to predict how the uncertainty of the pulsar mass may improve with further observations.

For each pulsar, we use our measured binary mass function and assume that the inclination angle is $i = 60^\circ$, which is the median for a uniform distribution. The pulsar masses, which heavily depend on the inclination angle, are poorly constrained in this scenario. Continued monitoring of these pulsars is therefore unlikely to constrain the fractional uncertainty to less than one third.

Using the χ^2 analysis in Shamohammadi et al. (2022, Section 4.1), we set $M_p = 1.2 M_\odot$ for PSRs J0900–3144, J1216–6410, and J1327–0755 to find the 16%, 50%, and 84% percentiles of $\cos i$, which are used to constrain the companion mass and the orbital inclination angle for each of these systems. We repeated the analysis for M_p equal to $2.0 M_\odot$. The results are shown in Table 3.

Based on the companion mass ranges obtained, we note the companion mass for PSR J0900–3144, $M_c > 0.38 M_\odot$ for all sampled values of pulsar mass, and at the lowest end of the pulsar mass range, i.e. at $M_p = 1.2 M_\odot$, the obtained mean value $\overline{M_c} = 0.60 M_\odot$. This mean value is larger than the typical mass associated with a He white-dwarf (WD) companion. We conclude that PSR J0900–3144 likely instead has a CO-WD companion (Tauris & Savonije 1999). In the case of PSR J1216–6410 we find that for the lowest pulsar mass, the associated $\overline{M_c} = 0.28 M_\odot$, typical of a He-WD companion. Even for a massive pulsar ($M_p = 2.0 M_\odot$), we have $\overline{M_c} = 0.42 M_\odot \lesssim 0.5 M_\odot$, the rough boundary mass above which instead a CO-WD is expected to form (Tauris & Savonije 1999). PSR J1216–6410 therefore likely has a He-WD companion. It is not possible to make a statement about the likely nature of the companion of PSR J1327–0755 since the M_c mass ranges associated with a light or heavy pulsar mass easily covers both He-WD and CO-WD solutions, and the mean values obtained for each simulated M_p lies close to the divide between He-WD and CO-WD masses.

Figure 3 indicates that these binary MSPs are required

Table 3. Constraints (central 68% confidence interval) on the companion star masses and inclination angles, assuming a pulsar masses of $1.2 M_\odot$ and $2.0 M_\odot$. For each system, the value of inclination angle presents an equally probable alternative solution of $180^\circ - i$.

Pulsar	M_p (M_\odot)	M_c (M_\odot)	$\cos i$	i°
J0900–3144	1.2	0.38–0.81	0.48–0.87	29–62
	2.0	0.55–1.13	0.54–0.88	28–58
J1216–6410	1.2	0.19–0.37	0.66–0.90	25–49
	2.0	0.29–0.54	0.72–0.91	24–44
J1327–0755	1.2	0.27–0.59	0.63–0.91	24–51
	2.0	0.40–0.85	0.69–0.92	23–47

to have $\cos i \leq 0.04$ to satisfy the condition of $\sigma_{M_p} \leq 0.1 M_\odot$. However, the ranges of $\cos i$ obtained from the χ^2 analysis show that all of these MSPs have $\cos i$ greater than 0.16. This shows that more observations of these systems will probably not improve the uncertainty of the pulsar mass.

6 CONCLUSION

We have updated the timing models for five MSPs using precision timing observations from the MeerKAT radio telescope. We account for noise processes in the timing residuals including pulse jitter, achromatic noise due to spin irregularities in the pulsars or gravitational waves, and dispersion measure variations in the ionised interstellar medium. For PSR J0900–3144 we identified a potential pulsar glitch at the beginning of 2023, but found no significant Bayesian evidence from our data supporting a glitch relative to a model of only red noise. We conclude that further observations are required to determine whether a glitch has occurred.

For PSR J0921–5202 we presented the first measurement of proper motion by combining the MeerKAT observations with earlier observations from Murriyang to increase the timing baseline. For all pulsars we use the proper motion measurements to derive transverse velocities (Table 2), using our derived distances from parallax measurements for PSRs J1216–6410, J1327–0755, and J1543–5149. We searched for a Shapiro delay in all of the pulsars and report weak detections for PSRs J0900–3144, J1216–6410, and J1327–0755. We were unable to derive useful constraints on the pulsar mass from these measurements, however, we discuss the likely ranges for the companion masses under assumed pulsar mass values. The companion of PSR J1216–6410 is likely a He-WD and PSR J0900–3144 likely CO-WD. We note that for these systems, future observations are unlikely to produce precise pulsar mass measurements from the Shapiro delay alone.

Finally, we presented the first detection of a clear Shapiro delay in PSR J1543–5149 and use it to derive a precise pulsar mass, $M_p = 1.349^{+0.043}_{-0.061} M_\odot$. The pulsar mass is unusually low for a recycled MSP. The birth mass is estimated to have been $M_p \sim 1.25 M_\odot$, making it one of the lightest neutron stars, and the lightest to have formed from the most common MSP formation channel.

DATA AVAILABILITY

The pulsar ephemerides, times of arrival, and noise models are available upon request from the corresponding authors. The observations are available from the MeerTime data portal, <https://pulsars.org.au/>.

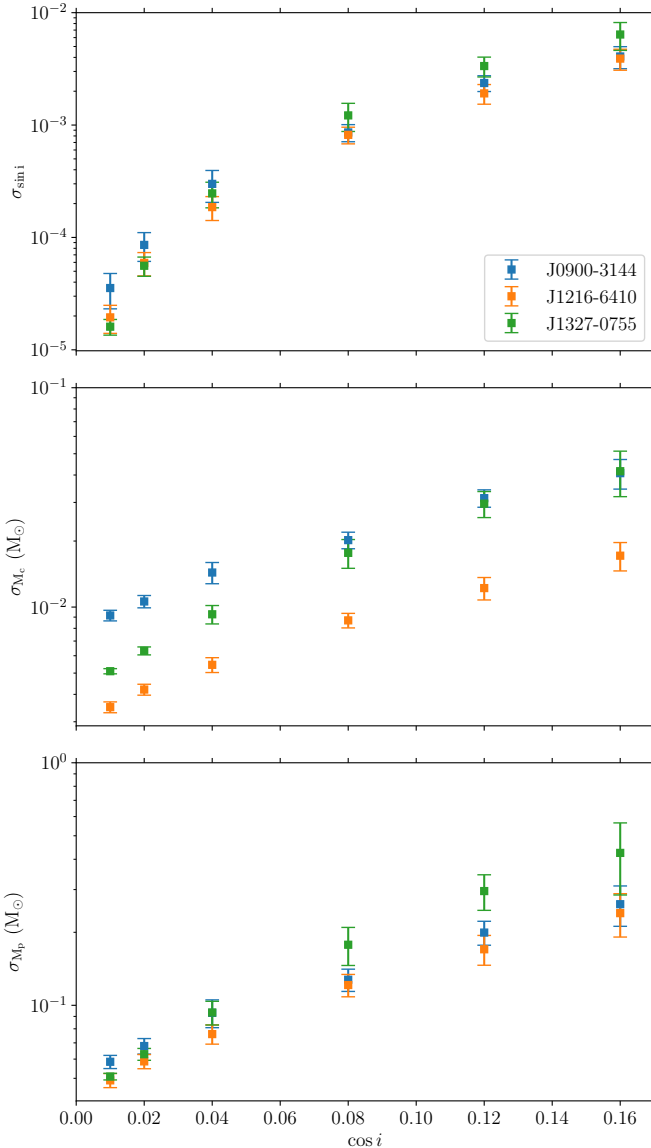


Figure 3. Change of uncertainties in $\sin i$ (top panel), M_c (middle panel), and M_p (bottom panel) as a function of $\cos i$ for PSRs J0900–3144, J1216–6410, and J1327–0755.

ACKNOWLEDGEMENTS

This research project was conducted as a student project, following an online MeerKAT pulsar timing workshop (<https://www.sarao.ac.za/e-learning-portal/>). We thank the organisers and contributors of the workshop and SARAO for its support. Funding was provided for the PTUSE machines by the Max-Planck-Institut für Radioastronomie (MPIfR), also supported by the MPG-CAS LEGACY programme, Swinburne University of Technology, and the Australian SKA office. This work was partially undertaken as part of the Australian Research Council Centre of Excellence for Gravitational Wave Astronomy (CE170100004 and CE23010016). MG acknowledges support from the South African Research Chairs Initiative of the DSI/NRF (grant No. 98626). Venkatraman Krishnan acknowledges financial support from the European Research Council (ERC) starting grant ‘COMPACT’ (grant agreement num-

ber:101078094). FA acknowledges that part of the research activities described in this paper were carried out with the contribution of the NextGenerationEU funds within the National Recovery and Resilience Plan (PNRR), Mission 4 – Education and Research, Component 2 – From Research to Business (M4C2), Investment Line 3.1 – Strengthening and creation of Research Infrastructures, Project IR0000034 – ‘STILES -Strengthening the Italian Leadership in ELT and SKA’.

REFERENCES

- Agazie G., et al., 2023, *ApJ*, **951**, L8
 Arzoumanian Z., et al., 2018a, *ApJS*, **235**, 37
 Arzoumanian Z., et al., 2018b, *ApJ*, **859**, 47
 Bailes M., et al., 2020, *Publ. Astron. Soc. Australia*, **37**, e028
 Barr E. D., et al., 2024, *Science*, **383**, 275
 Bhattacharya D., van den Heuvel E. P. J., 1991, *Physics Reports*, **203**, 1
 Boyles J., et al., 2013, *ApJ*, **763**, 80
 Burgay M., et al., 2006, *MNRAS*, **368**, 283
 Choudhury D., et al., 2024, *ApJ*, **971**, L20
 Cognard I., Backer D. C., 2004, *ApJ*, **612**, L125
 Cordes J. M., Lazio T. J. W., 2002, *arXiv e-prints*, pp astro-ph/0207156
 Cromartie H. T., et al., 2020, *Nature Astronomy*, **4**, 72
 Desvignes G., et al., 2016, *MNRAS*, **458**, 3341
 EPTA Collaboration et al., 2023, *A&A*, **678**, A50
 Edwards R. T., Hobson G. B., Manchester R. N., 2006, *MNRAS*, **372**, 1549
 Feroz F., Hobson M., Bridges M., 2009, *Monthly Notices of the Royal Astronomical Society*, **398**, 1601
 Fonseca E., et al., 2021, *The Astrophysical Journal Letters*, **915**, L12
 Foster R., Backer D., Wolszczan A., 1990, *The Astrophysical Journal*, **356**, 243
 Freire P. C. C., Wex N., 2010, *MNRAS*, **409**, 199
 Hotan A. W., van Straten W., Manchester R. N., 2004, *Publ. Astron. Soc. Australia*, **21**, 302
 Keith M. J., et al., 2011, *Monthly Notices of the Royal Astronomical Society*, **419**, 1752
 Kramer M., et al., 2021a, *Physical Review X*, **11**, 041050
 Kramer M., et al., 2021b, *MNRAS*, **504**, 2094
 Lange C., Camilo F., Wex N., Kramer M., Backer D., Lyne A., Doroshenko O., 2001, *Monthly Notices of the Royal Astronomical Society*, **326**, 274
 Lattimer J. M., Prakash M., 2004, *science*, **304**, 536
 Lattimer J. M., Prakash M., 2007, *Physics reports*, **442**, 109
 Lentati L., Alexander P., Hobson M. P., Feroz F., van Haasteren R., Lee K. J., Shannon R. M., 2014, *MNRAS*, **437**, 3004
 Lentati L., et al., 2016, *MNRAS*, **458**, 2161
 Lorimer D., et al., 2006, *Monthly Notices of the Royal Astronomical Society*, **372**, 777
 Lorimer D. R., et al., 2021a, *MNRAS*, **507**, 5303
 Lorimer D., et al., 2021b, *Monthly Notices of the Royal Astronomical Society*, **507**, 5303
 Lynch R. S., Freire P. C. C., Ransom S. M., Jacoby B. A., 2012, *ApJ*, **745**, 109
 McKee J. W., et al., 2016, *Monthly Notices of the Royal Astronomical Society*, **461**, 2809–2817
 Mickaliger M. B., et al., 2012, *The Astrophysical Journal*, **759**, 127
 Miles M. T., et al., 2023, *Monthly Notices of the Royal Astronomical Society*, **519**, 3976
 Miller M. C., et al., 2021, *The Astrophysical Journal Letters*, **918**, L28
 NANOGrav Collaboration et al., 2015, *ApJ*, **813**, 65
 Özel F., Freire P., 2016, *Annual Review of Astronomy and Astrophysics*, **54**, 401
 Park R. S., Folkner W. M., Williams J. G., Boggs D. H., 2021, *AJ*, **161**, 105
 Parthasarathy A., et al., 2021, *Monthly Notices of the Royal Astronomical Society*, **502**, 407
 Raaijmakers G., et al., 2021, *The Astrophysical Journal Letters*, **918**, L29
 Reardon D. J., et al., 2023a, *ApJ*, **951**, L6

- Reardon D. J., et al., 2023b, *ApJ*, **951**, L7
Reardon D. J., et al., 2024, *ApJ*, **971**, L18
Ridolfi A., Freire P. C. C., Gupta Y., Ransom S. M., 2019, *MNRAS*, **490**, 3860
Riley T. E., et al., 2021, *The Astrophysical Journal Letters*, **918**, L27
Serylak M., et al., 2022, *Astronomy & Astrophysics*, **665**, A53
Shamohammadi M., et al., 2022, *Monthly Notices of the Royal Astronomical Society*
Shamohammadi M., et al., 2024, *MNRAS*, **530**, 287
Shannon R. M., Cordes J. M., 2010, *The Astrophysical Journal*, **725**, 1607
Shapiro I. I., 1964, *Phys. Rev. Lett.*, **13**, 789
Spiewak R., et al., 2022, *Publ. Astron. Soc. Australia*, **39**, e027
Stovall K., et al., 2019, *ApJ*, **870**, 74
Tauris T. M., Savonije G. J., 1999, *A&A*, **350**, 928
Tauris T. M., Langer N., Kramer M., 2012, *MNRAS*, **425**, 1601
Xu H., et al., 2023, *Research in Astronomy and Astrophysics*, **23**, 075024
Yao J. M., Manchester R. N., Wang N., 2017, *ApJ*, **835**, 29
Zhu W. W., et al., 2015, *ApJ*, **809**, 41

This paper has been typeset from a $\text{\TeX}/\text{\LaTeX}$ file prepared by the author.